Structure of the Nucleoid-Associated Protein Cnu Reveals Common Binding Sites for H-NS in Cnu and Hha[†,‡]

Sung-Hun Bae,[§,||,⊥] Dinan Liu,[§,||] Heon M. Lim,[▽] Younghoon Lee,[§] and Byong-Seok Choi*[,§]

Department of Chemistry, KAIST, 373-1 Guseong-Dong Yuseong-Gu, Daejeon 305-701, Republic of Korea, and Department of Biology, School of Biological Science and Biotechnology, Chungnam National University, Daejeon, 305-764, Republic of Korea

Received September 19, 2007; Revised Manuscript Received December 7, 2007

ABSTRACT: Cnu is a nucleoid protein that has a high degree of sequence homology with Hha/YmoA family proteins, which bind to chromatin and regulate the expression of *Escherichia coli* virulence genes in response to changes in temperature or ionic strength. Here, we determined its solution structure and dynamic properties and mapped H-NS binding sites. Cnu consists of three α helices that are comparable with those of Hha, but it has significant flexibility in the C-terminal region and lacks a short α helix present in Hha. Upon increasing ionic strength, the helical structure of Cnu is destabilized, especially at the ends of the helices. The dominant H-NS binding sites, located at helix 3 as in Hha, reveal a common structural platform for H-NS binding. Our results may provide structural and dynamic bases for the similarity and dissimilarity between Cnu and Hha functions.

The YdgT gene was identified by open reading frame (ORF) analysis of the *Escherichia coli* genome (*1*) and predicted to encode a 71-amino acid protein that shares extensive sequence homology with members of the Hha/YmoA family of transcriptional regulatory proteins (Figure 1A). Hha has been shown to associate with the major nucleoid-associated protein H-NS (*2*); the bacterial nucleoid is an aggregated mass of DNA found in prokaryotic cells. Although the YdgT protein was also shown to bind to nucleoid-binding proteins H-NS and StpA (*3*), no definite cellular function has been assigned. Recently, Lim and co-workers (*4*) have found that YdgT as well as Hha forms a complex with H-NS and binds to *oriC*, the replication origin of *E. coli*, in an in vivo screening for novel proteins that bind to the replication origin; they named YdgT as Cnu for *oriC*-binding nucleoid-associated protein. In addition, Coombes and co-workers (*5*, *6*) have shown that YdgT and Hha exert negative regulatory activity on pathogenicity island-2 (SPI-2) in *Salmonella* in the absence of activating environmental signal.

Hha was initially identified in *E. coli* as a repressor of α-hemolysin expression (*7*). Synthesis of this toxin is repressed under conditions of either high osmolarity or low temperature, and mutations in the hha gene lead to derepression of the hemolysin expression when cells are grown either at low temperature or in a medium of high osmolarity (*8*). The YmoA from *Yersinia enterocolitica* shares 82% sequence similarity with the Hha and is a temperature-dependent repressor of the *yop* virulence gene (*9*, *10*). Mutations in both the *hha* and *ymoA* genes give rise to alterations in plasmid DNA supercoiling (*11*−*13*), and the two proteins are functionally interchangeable (*14*). Therefore, it has been suggested that Hha and YmoA are members of a class of proteins that modulate bacterial gene expression, probably by affecting DNA topology.

H-NS represses the expression of a variety of genes upon changes in osmolarity or temperature of the growth medium (*15*, *16*). DNA binding studies have shown that, in at least in vitro, Hha and H-NS together form a stable complex with DNA that differs from the protein−DNA complexes formed with either protein alone (*2*). H-NS forms a concentration-dependent, self-associated, high-order complex that binds preferentially to curved DNA (*17*, *18*) and induces bends in noncurved DNA (*19*). The interaction between Hha and H-NS does not require the presence of DNA and is impaired by high concentrations of KCl (∼1 M) (*2*, *20*). H-NS consists of an N-terminal oligomerization domain and a C-terminal DNA binding domain that are separated by a long flexible linker, which enables the C-terminal domain to move freely relative to the N-terminal domain (*17*, *21*−*23*). Although it has been reported that residues 1−89 of H-NS are necessary and sufficient for high-order oligomerization and a truncated version of the N-terminal oligomerization domain (residues 1−57 or 1−64) forms a defined homodimer (*24*, *25*), the precise oligomeric state of full-length or truncated H-NS has not been elucidated yet. Solution structures of the N-terminal domains have revealed that the oligomerization domain consists of three α helices and forms a homodimer in either parallel (*24*) or antiparallel (*26*, *27*) orientation.

Cnu shares amino acid sequence homology with, and displays an H-NS binding affinity comparable to those of, Hha and YmoA. Furthermore, Cnu and Hha appear to

[†] This work was supported by the National Creative Research Initiative from the Ministry of Science and Technology of the Republic of Korea.

[‡] Coordinates described in this paper have been deposited in the Protein Data Bank (PDB code: 2JQT).

* Corresponding author: phone +82-42-869-2828; fax +82-42-869-8120; e-mail byongseok.choi@kaist.ac.kr.

[§] KAIST.

[||] These authors contributed equally to this work.

[⊥] Present address: Department of Molecular Biology, The Scripps Research Institute, 10550 North Torrey Pines Rd., La Jolla, CA 92037.

[▽] Chungnam National University.

10.1021/bi701914t CCC: $40.75
Published on Web 01/12/2008

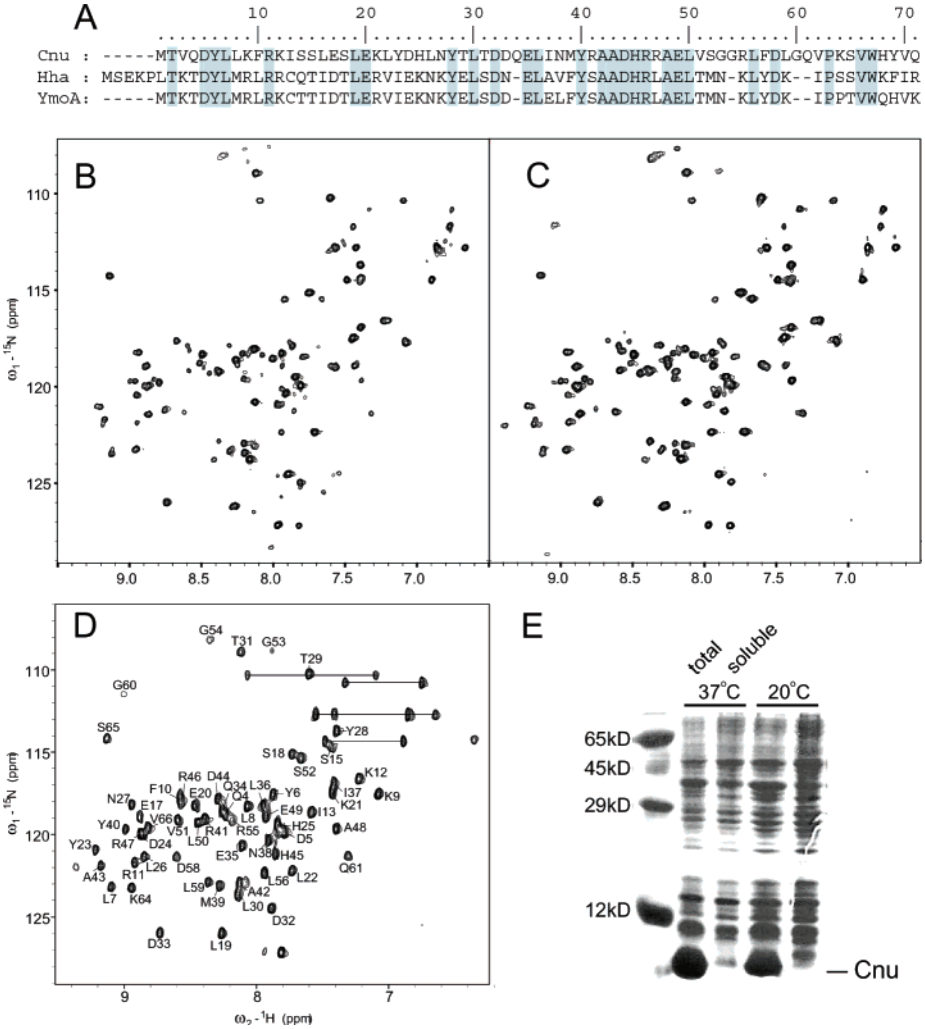

FIGURE 1: In vitro refolding. (A) Sequence alignment of Cnu, Hha, and YmoA. Residue numbering is based on Cnu. Identical sequences are indicated by gray box. (B, C) $^{1}H-^{15}N$ HSQC of (B) solubly expressed and (C) in vitro refolded Cnu. (D) $^{1}H-^{15}N$ HSQC assignment of Cnu. Horizontal lines are side-chain amino proton resonances. Unassigned peaks showed no sequential connectivity in 3-D CBCA(CO)NH, 3-D HNCACB, or 3-D ^{15}N-edited NOESY-HSQC. (E) Total and soluble fractions of intact Cnu overexpressed at 37 and 20 °C.

compensate for each other in some cases (*4*−*6*). So, in order to decipher the common structural features and possible differences between Cnu and Hha, we characterized the solution structure and dynamics of Cnu and the Cnu−H-NS interaction by NMR[1] spectroscopy. Cnu has three α helices that have a conformation very similar to those of Hha, but it lacks the C-terminal short helix present in Hha due to high flexibility. These helical structures were destabilized at increased ionic strength, suggesting a possible mechanism for the ionic strength sensitivity. In vitro binding assays and NMR relaxation measurements showed that the H-NS binding sites of Cnu include the flexible C-terminal region and they are mostly overlapped with H-NS binding sites of Hha. The dominant H-NS binding sites, located at helix 3 as in Hha, reveal a common structural platform for H-NS binding. Our results may provide structural and dynamic bases for the similarity and dissimilarity between Cnu and Hha functions.

MATERIALS AND METHODS

Cloning and Expression of Cnu. A polymerase chain reaction- (PCR-) amplified *Cnu* gene was inserted into the *Nde*I/*Xho*I sites of pET-28a (Novagen) for intact Cnu or into the *Nde*I/*Bam*HI sites of pET-15b (Novagen) for Cnu carrying an N-terminal histidine tag (His-Cnu). Cloned vectors were transformed into *E. coli* BL21(DE3) or BL21-(DE3)pLysS cells and grown at 37 °C in either Luria−Bertani (LB) or M9 minimal medium containing $^{15}NH_4Cl$ (1 g/L) and ^{13}C-glucose (2 g/L) (*28*). Overexpression of the Cnu proteins was induced by 0.4 mM IPTG when cells reached an OD_{600} of ∼0.7. Cells were grown at 37 °C for an additional 4−6 h.

In Vitro Refolding and Purification of His-Cnu. After cell lysis, the aggregated cell pellet was washed twice with 20 mM sodium phosphate (pH 7.3), 0.2 M NaCl, and 1% Triton X-100 and dissolved in 40 mM sodium phosphate (pH 7.3), 0.4 M NaCl, and 6 M guanidine hydrochloride. The chemically denatured protein was loaded on a Ni-NTA

[1] Abbreviations: NMR, nuclear magnetic resonance; CD, circular dichroism; HSQC, heteronuclear single quantum correlation; hnNOE, heteronuclear Overhauser effect; R_2 (=$1/T_2$), transverse relaxation rate; IPTG, isopropyl β-D-thiogalactoside; NTA, nitrilotriacetate; SDS, sodium dodecyl sulfate; COSY, correlation spectroscopy; TOCSY, total correlation spectroscopy; NOESY, nuclear Overhauser effect spectroscopy; EMSA, electrophoretic mobility shift assay.

column, which was pre-equilibrated with binding buffer [50 mM sodium phosphate buffer (pH 8.0), 8 M urea, and 5 mM imidazole]. After sample loading, the column was washed with the binding buffer and washing buffer [50 mM sodium phosphate buffer (pH 8.0), 8 M urea, 20 mM imidazole, and 0.15 M NaCl]. The protein was refolded in the column by rinsing the column with refolding buffer [50 mM sodium phosphate buffer (pH 8.0), 1 M urea, 20 mM imidazole, 0.5 M NaCl, and 2 mM $MgCl_2$] and 50 mM sodium phosphate (pH 8.0) and 0.5 M NaCl. Refolded protein was then digested by thrombin and eluted from the column by the binding buffer. The refolded and digested Cnu was further purified and exchanged to NMR buffer [20 mM sodium phosphate (pH 7.5)] by use of a Superdex 75 16/60 column (Amersham Biosciences). Tightly bound Mg^{2+} was not found in the prepared Cnu samples as analyzed by the ICP-MS (inductively coupled plasma mass spectrometry) and $^{1}H-^{15}N$ HSQC (Bruker 800 and 900 MHz spectrometers). Cnu concentration was determined by UV absorbance at 280 nm (1 mM = 12.2 OD_{280}/mL).

Expression and Purification of H-NS. The H-NS expression plasmid, pHOP11, was transformed into *E. coli* BL21 cells. H-NS was purified according to the previously described method (*29*, *30*) with slight modifications. After cell lysis, the supernatant was precipitated by 40% (w/v) ammonium sulfate, dissolved in 50 mM sodium phosphate (pH 7.0) and 1.0 M ammonium sulfate, and loaded onto a phenyl-Sepharose FF column (Amersham Biosciences) equilibrated with the same buffer. Protein was eluted with 50 mM sodium phosphate (pH 7.0) and dialyzed against Mono-S binding buffer [10 mM sodium phosphate (pH 7.0)]. Dialyzed protein was loaded onto a Mono-S 10/10 column (Amersham Biosciences) that had been equilibrated with Mono-S binding buffer and eluted with NaCl gradient.

Circular Dichroic Spectroscopy. CD was measured at room temperature on a Jasco J-720 spectropolarimeter. Far-UV wavelength scans were recorded from 350 to 200 nm, with resolution of 0.2 nm, a speed of 50 nm/min, a response time of 2 s, and a bandwidth of 2 nm. Spectra were collected and averaged over 10 scans.

In Vitro Binding Assay with Ni-NTA Agarose. A 50% slurry of Ni-NTA agarose (100 μL, Qiagen) was equilibrated with 50 mM sodium phosphate (pH 8.0), 0.5 M NaCl, 5 mM imidazole, and 0.1% Triton X-100. Cnu was mixed with either H-NS(1−57) or H-NS(1−89) with an N-terminal histidine tag, and the reaction mixture was incubated with Ni-NTA agarose resin for 30 min at 4 °C. Unbound proteins were removed from the resin by washing, and the bound proteins were then eluted with buffer containing 1.0 M imidazole. Unbound, washed, and eluted fractions were analyzed on a 12% tricine−SDS−polyacrylamide gel and stained by Coomassie blue.

NMR Resonance Assignments and Structure Calculation. All NMR experiments were carried out at 25 °C on a Varian Unity Inova 600 MHz spectrometer. NMR samples containing 0.4−0.8 mM ^{15}N- or $^{15}N/^{13}C$-labeled Cnu in 20 mM sodium phosphate (pH 7.5), 90% H_2O/10% D_2O were prepared for 2-D ^{15}N HSQC and 3-D CBCA(CO)NH, HNCACB, HNCO, HCCH-COSY, HCCH−TOCSY, (H)CCH−TOCSY, HBHA(CO)NH, ^{13}C-edited NOESY-HSQC and ^{15}N-edited NOESY-HSQC experiments (*31*). Acquired spectra were processed with NMRPipe (*32*) and analyzed with Sparky 3.1 (*33*). For structure calculations, distance restraints were derived from NOE cross-peaks in the ^{15}N-edited NOESY-HSQC and ^{13}C-edited NOESY-HSQC spectra, and dihedral angle restraints were obtained from chemical shift analysis by use of TALOS (*34*). Initial structure calculation which combined automated NOE cross-peak assignment was achieved by CYANA (*35*). The resulting NOE assignment and distance restraints were manually confirmed and used for further structure calculations by CNS (*36*). In CNS calculation, an extended coil used for starting structure was subjected to 15 ps of torsion angle dynamics at 50 000 K, followed by 15 ps of torsion angle dynamics cooling to 0 K and 15 ps of Cartesian dynamics cooling from 2000 to 0 K. The final structures were generated after 2000 cycles of energy minimization. The distance force constant was 150 kcal·mol^{-1}·Å^{-2} and the dihedral angle force constant, which initially was 100, was scaled to 200 kcal·mol^{-1}·radian^{-2} during cooling. Twenty-three out of 100 trial structures were converged, and the 10 lowest energy conformers were selected for final analysis. Coordinates are deposited in the Protein Data Bank (PDB code: 2JQT).

Dynamics and Binding Site Mapping by NMR. The $[^{1}H]-^{15}N$ NOE (hnNOE) was measured with a 3 s saturation or a 3 s delay without saturation (*37*). hnNOE values were determined as the ratios of the peak intensities measured from spectra acquired with and without saturation during repetition delay (*38*). ^{15}N-labeled Cnu was titrated with unlabeled H-NS to Cnu:H-NS molar ratios from 1:0.01 to 1:14.5 in which the Cnu concentration was ∼10−45 μM. The average chemical shift change ($\Delta\delta_{avg}$) combining ^{1}H and ^{15}N dimensions was calculated from an empirical equation, $[(\Delta\delta^{1}H)^2 + 0.2(\Delta\delta^{15}N)^2]^{1/2}$. ^{15}N R_2 relaxation rates were measured at eight R_2 delays (t = 10, 30, 50, 70, 90, 110, 150, and 230 ms). Peak intensities (I) were fitted to a single-exponential decay function, $I = I_0e^{-R_2t}$. The repetition delay was 2 s. The R_2 relaxation rates of Cnu in the presence and absence of H-NS were measured at molar ratio 1:3 (Cnu:H-NS).

RESULTS

In Vitro Refolding. Intact and N-terminal histidine-tagged Cnu (His-Cnu) formed insoluble aggregates when overexpressed (Figure 1E). However, they could be refolded in vitro, with an average efficiency of 75−90%. Although His-Cnu that was overexpressed in bacteria existed mostly in the insoluble fraction, ∼5% of His-Cnu was found in the soluble fraction (Figure 1E), and this soluble protein was used to examine whether in vitro refolded Cnu has the same conformation as the inherently soluble Cnu. The ^{15}N-HSQC spectrum of inherently soluble Cnu prepared from a 2-L bacterial culture was compared with that of in vitro refolded Cnu. All cross-peaks in the ^{15}N-HSQC spectra of the inherently soluble (Figure 1B) and in vitro refolded (Figure 1C) proteins completely match each other, indicating that the in vitro refolded protein has the same conformation as the inherently soluble counterpart.

NMR Resonance Assignments. Cnu was stable for several months at 25 °C in 20 mM sodium phosphate (pH 7.5), as monitored by NMR. Sequential assignments of ^{1}H, ^{13}C, and ^{15}N backbone resonances were achieved by using three-dimensional (3-D) CBCA(CO)NH, 3-D HNCACB. Intraresidue and sequential correlations between resonances of HN(i),

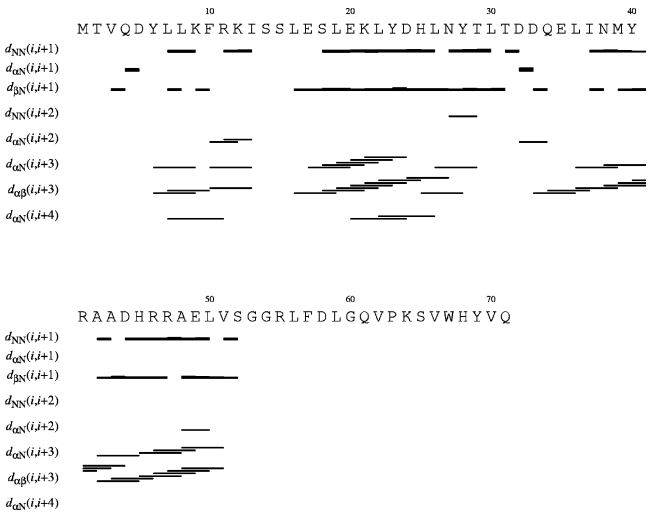

FIGURE 2: NOE connectivities. The thickness of lines reflects the intensity of NOE. NMR experiments were carried out at 25 °C with 0.4−0.8 mM ^{15}N- or ^{15}N/^{13}C-labeled Cnu samples in 20 mM sodium phosphate (pH 7.5), 90% H_2O/10% D_2O.

Table 1: Statistics for Cnu Structure Determination

no. of distance constraints	401
intraresidue	147
medium-range ($1 \geq |i-j| \geq 4$)	196
long-range ($|i-j| > 4$)	28
hydrogen bonds	30
no. of dihedral angle constraints	96
distance constraints violations (>0.5 Å)	0
dihedral angle constraints violations (>5°)	0
mean deviation from ideal covalent geometry	
bond length (Å)	0.00067
bond angle (deg)	0.298
improper angle (deg)	0.09
Ramachandran analysis[a]	
most favored regions (%)	87.4
additional allowed regions (%)	11.9
generously allowed regions (%)	0.8
disallowed regions (%)	0.0
pairwise rmsd of residues 6−52	
backbone atoms (N, Cα, and C) (Å)	0.82 ± 0.12
all heavy atoms (Å)	1.84 ± 0.15

[a] Ramanchandran analysis was performed by using PROCHECK-NMR (*50*).

N(i), and Cα(i)−Cβ(i) or Cα(i − 1)−Cβ(i − 1) in 3-D HNCACB could be resolved with 3-D CBCA(CO)NH, which contains only sequential correlations. Carbonyl carbon resonances were assigned with 3-D HNCO and the side-chain ^{1}H and ^{13}C resonances were assigned by 3-D HCCH-COSY, HCCH-TOCSY, (H)CCH-TOCSY, HBHA(CO)NH, ^{13}C-edited NOESY-HSQC, and ^{15}N-edited NOESY-HSQC. All residues were sequentially assigned except for some C-terminal residues (V62, P63, and W67−Q71) (Figure 1D) which did not show sequential connectivities due to flexibility. The stretches of nonsequential αN(i, i + 3), αN(i, i + 4), αβ(i, i + 3) and strong sequential NN NOE connectivities in the ^{15}N-edited NOESY-HSQC and ^{13}C-edited NOESY-HSQC showed the presence of three helical segments of Cnu (Figure 2).

Solution Structure. A total of 401 distance constraints and 96 dihedral angle constraints obtained from NMR measurements were used to calculate the solution structure by using CYANA (*35*) and CNS (*36*). Twenty-three out of 100 extended starting structures were converged and the 10 lowest energy conformers were selected for final analysis in which the pairwise root-mean-square deviation (rmsd) of residues 6−52 for backbone atoms is 0.82 ± 0.12 Å and for all heavy atoms is 1.84 ± 0.15 Å (Table 1 and Figure 3A). Secondary structure analysis of the obtained structures identified three α helices (Y6−K12, E17−T29, and D33−V51) forming a bundle in which hydrophobic residues are clustered at the interfaces between the helices (Figure 3B). Especially, five repeated L(x)$_{2-3}$L motifs in helix 2 (Figure 1A) make the inner face of the helix hydrophobic and the outer face of the helix hydrophilic, which should facilitate bundle formation. As expected from the high degree of sequence similarity between Cnu and Hha, overall structure of Cnu is similar to that of Hha such that the rmsd of Cα atoms between helices 1−3 of Cnu and Hha is 2.0 Å (Figure 3C). However, Cnu lacks a stable secondary structure following helix 3, while Hha has a short helix 4 that interacts with the C-terminal end of helix 3. The highly conserved R46 of Cnu forms a hydrogen bond with backbone carbonyl groups of I13 and S14, which connect helices 1 and 2. In addition, there are extensive network of polar contacts at the linker between helices 2 and 3 (T29•L30, T29•L26, Y28•T31, D32•D33, D32•Q34, and D32•E35) that stabilize the linker.

C-Terminal Flexibility. To verify that the lack of helix 4 in Cnu structure is caused by flexibility of the C-terminal region, the [^{1}H]−^{15}N heteronuclear Overhauser effects (hnNOE) were measured (Figure 3D). By use of this technique, flexible regions such as surface-exposed loops are readily distinguishable from the folded protein core since the flexible or unfolded parts yield low or negative hnNOEs (*37*). Most Cnu residues exhibited hnNOEs of around 0.8−0.9, indicating rigidly folded structure. On the other hand, the C-terminal residues had much lower hnNOEs (0.3−0.6), which shows that the C-terminal region is highly flexible on a pico- to nanosecond time scale. In accordance with this result, the ^{15}N transverse relaxation rates (R_2) of the C-terminal residues are more divergent and smaller ($R_2 \sim 6-9$ s^{-1}) than in other parts of the molecule ($R_2 \sim 9-10$ s^{-1}) (Figure 3D). Therefore, the presence or absence of helix 4 in Hha and Cnu is attributed to the differential dynamics of the C-terminal region.

Destabilization of Helix Structure at Elevated Ionic Strength. Since the homologous Hha/YmoA family proteins respond to changes of ionic strength, conformational change of Cnu in the presence of divalent metal ions was monitored by circular dichroism (CD) and NMR (Figure 4A−C). In the absence of metal ions (buffer), Cnu showed a typical CD profile of α helices. However, the absolute CD intensity in the far-UV (200−230 nm) region was dramatically reduced in the presence of various divalent metal ions. Since the far-UV region is very sensitive to the structural content of the α helix, β strand, and random coil, this data clearly shows that α-helical content of Cnu decreases at increased ionic strength in a metal-ion-dependent manner, according to the following order: $Ca^{2+} > Zn^{2+} > Mn^{2+} > Mg^{2+} \gg Co^{2+} > Ni^{2+} > Cu^{2+}$. Residues whose ^{15}N HSQC peaks were substantially perturbed by addition of Mg^{2+} resided mostly at the N- and/or C-terminal ends of the three helices (Q4, H25, Y28, T29, D32, Q34, H45, E49, G60, and K64) (Figure 4B−D). These residues are located at the molecular surface and more exposed to solvent than any other regions of the

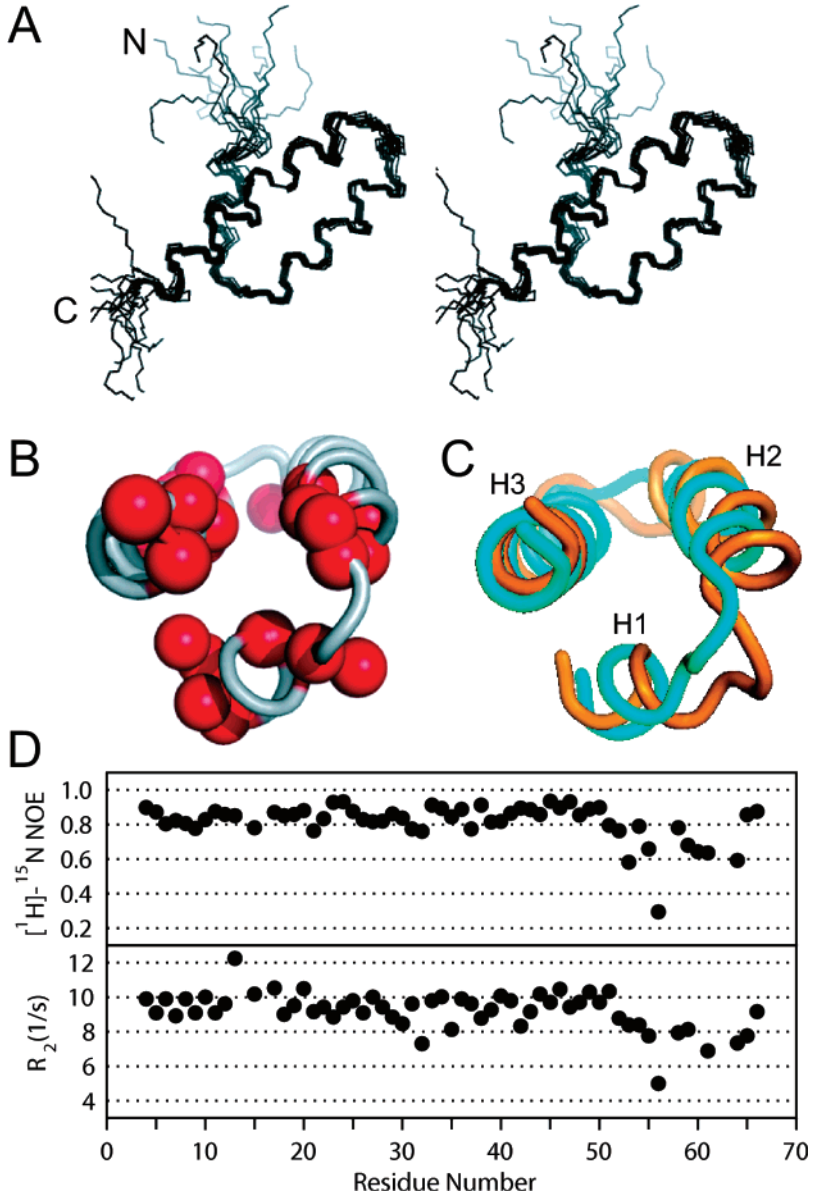

FIGURE 3: Structure and dynamics. (A) Stereoview showing best-fit superposition of backbone heavy atoms of residues 1−57. The atomic coordinates have been deposited in the Protein Data Bank (PDB code 2JQT) (B) Cα atoms of hydrophobic residues shown as red spheres on the coil representation of helices 1−3. (C) Structural comparison between helices 1−3 of Cnu (cyan) and those of Hha (orange, PDB code 1JW2). (D) [^{1}H]−^{15}N NOE and ^{15}N R_2 relaxation rates of Cnu.

protein. Most of those residues are also involved in hydrogen bonding or polar contacts in the determined structure. It has been known that specific patterns of hydrogen bonding and hydrophobic interactions (the so-called helix capping motifs) found at or near the ends of α helices stabilize helix structure in proteins (*39*). Since the hydrogen bonds are more easily disrupted at high ionic strength, the response to ionic strength of Cnu and Hha/YmoA proteins might be understood by the conformational changes following disruption of the stabilizing hydrogen bonds or polar contacts at the ends of the helices in addition to the osmolarity-modulated gene expression mechanism, which is supported by the finding that increasing the osmolarity of LB medium had no significant effect on the Hha gene expression whereas depletion of NaCl led to a significant decrease of gene expression (*40*).

Interaction with H-NS. Hha binds tightly to H-NS in vitro (*20*), and it was recently confirmed that Cnu also binds to H-NS and its paralogue StpA in vitro (*3*). To characterize the interaction between Cnu and H-NS in detail, we performed a series of ^{15}N-HSQC experiments in which unlabeled full-length H-NS was added to ^{15}N-labeled Cnu in molar ratios of 1:0.01 to 1:14.5 (Cnu:H-NS). Even at the high molar ratios, chemical shift perturbations of Cnu by the addition of H-NS were not large enough to clearly identify the binding sites ($\Delta\delta_{avg}$ <0.04 ppm) (data not shown). Therefore, to identify the H-NS binding sites in Cnu, we measured the ^{15}N R_2 relaxation rates of Cnu in the presence and absence of H-NS because the R_2 relaxation rates of binding sites would increase by slower local tumbling or by chemical exchange between bound and free states (*41*). The R_2 ratio (R_2[Cnu + H-NS]/R_2[Cnu alone]) showed that the R_2 rates of Q4, L8−F10, I13, E17, L19, N27, E35, L36, M39−H45, L56, L59, K64, and V66 are significantly increased by H-NS binding (Figure 5A,B). Interestingly, these H-NS binding regions are partly overlapped with the regions whose chemical shifts are perturbed by addition of Mg^{2+}, suggesting that H-NS binding might modulate Cnu's sensitivity to ionic strength. In addition, most of these

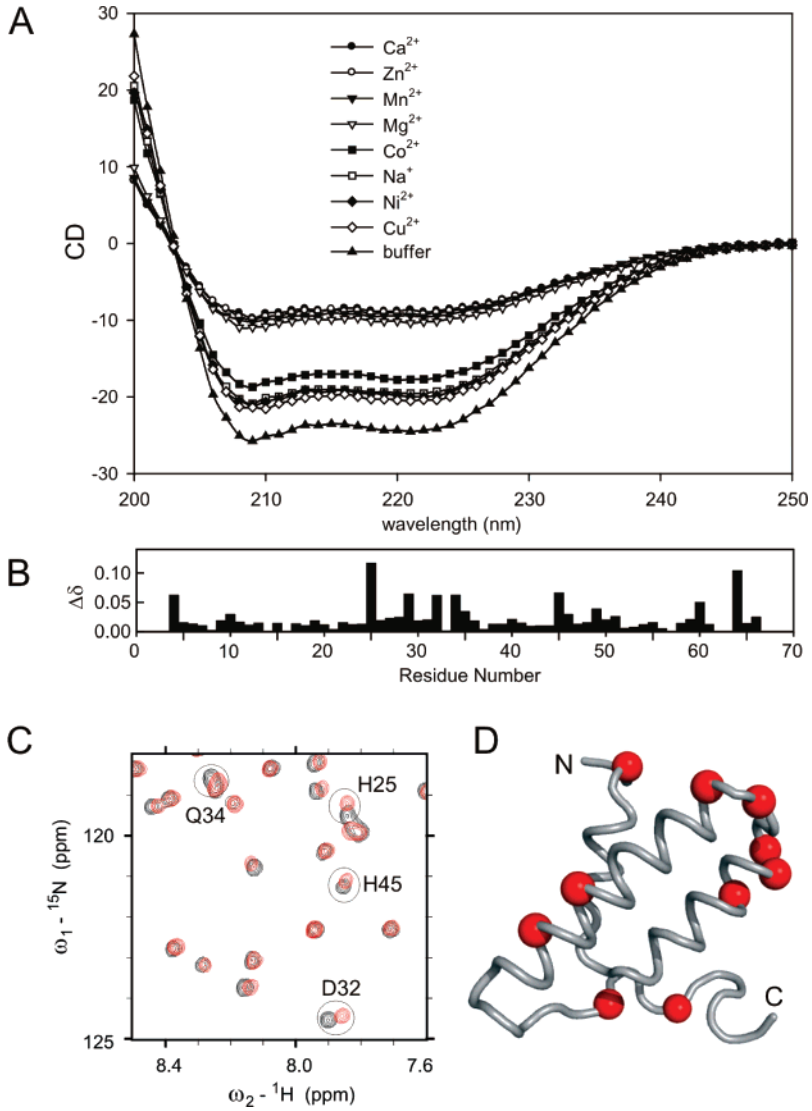

FIGURE 4: Destabilization of helices at increased ionic strength. (A) CD spectra in the presence and absence of metal ions. $CaCl_2$, $ZnCl_2$, $MnCl_2$, $MgCl_2$, $CoCl_2$, NaCl, $NiSO_4$, and $CuSO_4$ were added to Cnu (30 μM) in 10 mM sodium phosphate (pH 8.0) buffer. All salt concentrations were 1 mM except for NaCl (100 mM). The ionic strength of $NiSO_4$ or $CuSO_4$ is $^4/_3$ that of other chloride salts when complete ionization is assumed. (B) Chemical shift changes in the presence and absence of Mg^{2+}. $^1H-^{15}N$ HSQC spectra were measured at 25 °C with about 0.4 mM ^{15}N-labeled Cnu samples in 20 mM sodium phosphate (pH 7.5), 90% H_2O/10% D_2O in the presence and absence of 16 mM $MgCl_2$. The average chemical shift change ($\Delta\delta$) combining ^1H and ^{15}N dimensions was calculated from an empirical equation, $[(\Delta\delta^1H)^2 + 0.2(\Delta\delta^{15}N)^2]^{1/2}$. (C) A $^1H-^{15}N$ HSQC region highlighting H25, D32, Q34, and H45 whose chemical shifts are significantly changed by Mg^{2+}. Peak contour lines are colored in black and red for the absence and presence of Mg^{2+}, respectively. (D) Residues showing the most significant chemical shift changes by Mg^{2+} are depicted as red spheres on the ribbon representation of the Cnu structure.

residues are well overlapped with the Hha residues whose NMR peaks were broadened by binding to H-NS(1−64) (residues in helices 1, 3, and 4 of Hha) (*42*). The stretches of conserved residues among Cnu and Hha/YmoA family proteins including the most conserved sequence, [R/S]-AADHR (residues 41−46 of Cnu), are clustered in helix 3 (Figure 1A) and broadened by H-NS binding in both Cnu and Hha (*42*) to a greater extent than other residues, revealing a common structural platform for H-NS binding.

The oligomerization domain of H-NS (1−64), which forms a homodimer (*24*), was shown to interact with Hha by fluorescence anisotropy and NMR (*42*), and full-length H-NS was shown to bind Cnu (*3*). Herein, we used Ni^{2+}-NTA agarose-based in vitro binding assays to examine whether two versions of N-terminal domains of H-NS (1−57 and 1−89) bind to Cnu. Both H-NS constructs bound to Cnu in vitro (Figure 5C,D), even under high-salt conditions (0.5 M NaCl), suggesting that the H-NS(1−57) is sufficient for Cnu binding. In addition, gel-filtration chromatography experiments show that H-NS(1−57) and Cnu form a 2:1 complex (Table 2), which is consistent with the fluorescence anisotropy results obtained for the Hha−H-NS(1−64) complex (*42*). However, chemical shift perturbations of ^{15}N-labeled H-NS(1−57) in the presence and absence of unlabeled Cnu were too small to identify the Cnu binding sites of H-NS-(1−57) (data not shown), which is probably caused by dominant H-NS(1−57)/H-NS(1−57) interactions.

DISCUSSION

In general, bacterial transcriptional repressors block RNA polymerase's access to the gene promoter either by physically occupying that promoter site or by altering local DNA

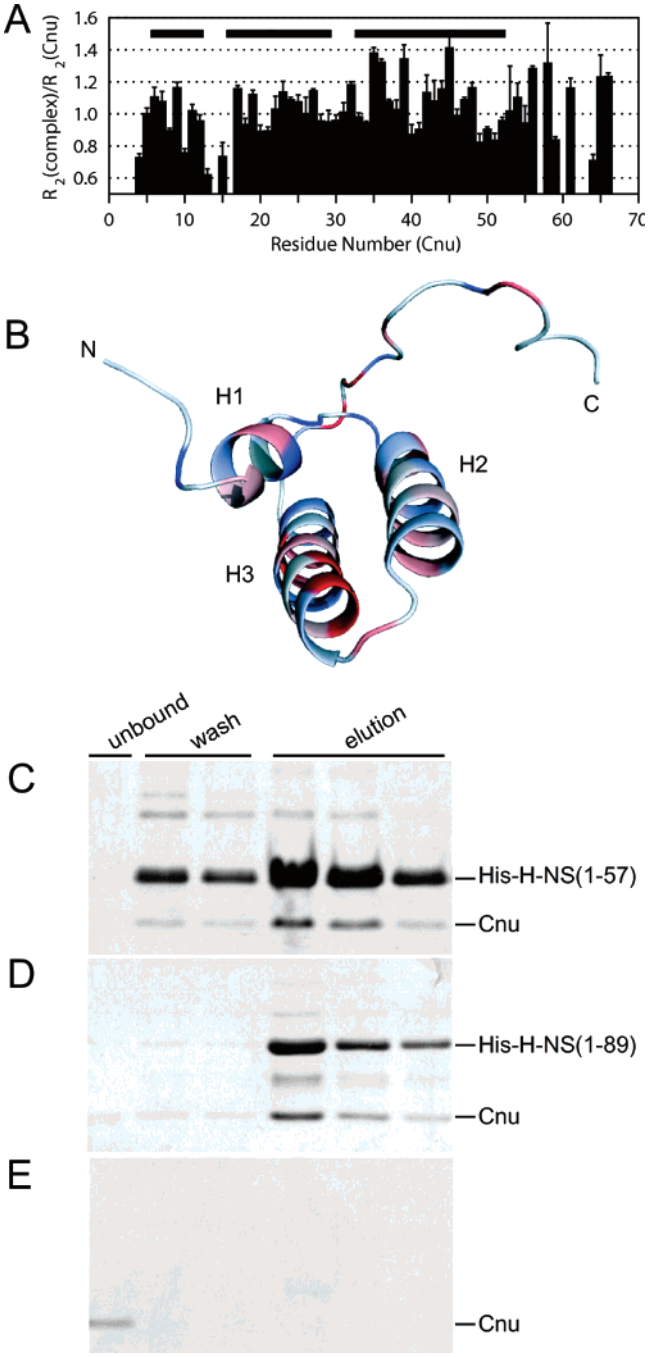

FIGURE 5: Interaction with H-NS. (A) ^{15}N R_2 relaxation rate changes of Cnu upon H-NS binding. Helices 1−3 of Cnu are indicated by boxes. (B) ^{15}N R_2 relaxation rate changes, as in panel A, are mapped on the ribbon representation of Cnu by color spectrum in which the smallest and largest ratios are shown in blue and red, respectively. (C−E) In vitro binding assays for Cnu and histidine-tagged H-NS (His-H-NS). Unbound, washed, and eluted fractions were analyzed by 12% tricine−SDS−PAGE and stained by Coomassie blue. (C) Cnu and H-NS(1−57). (D) Cnu and H-NS-(1−89). (E) Cnu alone (control).

topology. Hha/YmoA proteins participate in the transcriptional repression of virulence genes in response to environmental changes like temperature and osmolarity. Hha binds to its regulatory site in the hemolysin gene operon (*hlyM*), but its affinity and specificity for this site are even weaker than those of H-NS for nonspecific binding to this site (*2*). So, it is intriguing that Hha must bind to H-NS in order to form a ternary complex with the *hlyM* DNA. This ternary complex differs from the DNA−protein complexes formed with Hha or H-NS alone, although Hha does not appear to enhance the DNA binding affinity or specificity of H-NS (*2*).

Table 2: Gel-Filtration Chromatography of the Cnu/H-NS(1−57) Complex[a]

protein	elution time (min)	molecular mass (kDa)
Cnu[b]	90.82	7.6 (8.7)[c]
cytochrome *c*	82.68	12.4
Cnu[b] + His-H-NS$_{1-57}$[d]	69.83	27.7 (26.3)[c,e]
carbonic anhydrase	69.77	29
ovalbumin	61.44	45
bovine serum albumin	55.80	66

[a] A Superdex 75 16/60 column (Amersham Biosciences) was run with 20 mM sodium phosphate (pH 7.3) and 200 mM NaCl at a flow rate of 1 mL/min. [b] Cnu was prepared by thrombin digestion of His-Cnu and contains an additional NH_2-GSHM- sequence. [c] For Cnu and His-H-NS(1−57) + Cnu, the hydrodynamic molecular mass is shown with the predicted molecular mass in parentheses. [d] His-H-NS contains an additional NH_2-GSSHHHHHHSSGLVPRGSHM- sequence. [e] The molecular mass was predicted for a 2:1 complex of His-H-NS and Cnu.

In contrast to Hha, which has a dissociation constant (K_d) in the micromolar range for DNA (*2*), Cnu alone does not appear to bind DNA, as was observed in our EMSA and NMR experiments (data not shown). At best, Cnu might have a K_d in the high millimolar range for DNA, which is outside our detection limit and would be irrelevant to the actual biological system. Nevertheless, Cnu showed highly sequence-specific DNA binding in in vivo assays, such that a single nucleotide mutation in the Cnu binding site (*oriC*) could disrupt Cnu−*oriC* association (*4*). These findings strongly imply that the *oriC* binding activity of Cnu is dependent on complex formation with H-NS, although an unknown specificity factor cannot be excluded. In addition to the Cnu and Hha/YmoA proteins, H-NS interacts with many other proteins, including the gene 5.5 product of bacteriophage T7 (*43*), the RNA binding protein HF-I (*44*), the H-NS analogue StpA (*45*), and the flagellar rotor protein FliG (*46*). However, the nature of the interaction between these proteins and H-NS has not been characterized at the molecular level, partly because H-NS undergoes a high degree of self-oligomerization. H-NS alone forms a concentration-dependent oligomer through its N-terminal oligomerization domain and interdomain linker. It has been shown in one study that the minimal oligomeric state of H-NS is a dimer and the higher oligomers are nonspecific aggregates (*26*). However, another recent report argues that a tetramer is the minimum functional form of H-NS in vivo (*47*). On the basis of sequence homology between Cnu, Hha/YmoA, and the N-terminal region of H-NS (*20*), it has been proposed that the H-NS residues involved in the H-NS dimer interface can be replaced with a new binding partner, either Cnu or a Hha/YmoA protein (*48*). This domain swapping would generate a complex where the homologous residues within Cnu or Hha/YmoA locate at the interface with H-NS. However, in our gel-filtration chromatography experiments, the H-NS dimer was not disrupted in vitro, even in the presence of excess amounts of Cnu (data not shown). This observation suggests that (i) the affinity between two H-NS molecules is much stronger than the affinity between H-NS and Cnu, and thus (ii) the H-NS−Cnu complex consists of at least two molecules of H-NS, which is consistent with the gel-

filtration chromatography data for the Cnu-H-NS(1−57) complex (Table 2) and fluorescence anisotropy data for the Hha-H-NS(1−64) complex (*42*).

The overall structures of Cnu and Hha are very similar except for the C-terminal region. In accordance with this structural similarity, H-NS binding sites of these two proteins are also similar. Interestingly, the C-terminal residues of Cnu, which are very flexible and do not form a stable helix, are also engaged in H-NS binding (Figure 5A), while the same residues in Hha, which are involved in H-NS binding, form a stable short helix (*42*, *49*). So, a particular three-dimensional structure of the C-terminal region may not be necessary for H-NS binding, or the C-terminal region might have different H-NS binding modes in Cnu and Hha. For a 1:1 complex with H-NS at 25 °C, Hha showed severe line broadening of all peaks due to chemical exchange in the intermediate time regime (*42*). Under the same conditions, Cnu also displayed some line broadenings upon H-NS binding that were detected by the increase of R_2 (Figure 5A); however, these line broadenings are much less severe and not observed for all residues. These different NMR characteristics between Cnu and Hha could be understood by the differential time scale underlying the association and dissociation with H-NS. Hha−H-NS interaction appears to occur on the intermediate NMR time scale, while Cnu−H-NS interaction occurs on the faster NMR time scale. The different flexibility and structure of the C-terminal region, if not exclusively, may provide unique H-NS binding kinetics for Cnu and Hha so that under certain conditions they might differentially respond to environmental factors such as protein concentration, ionic strength, and temperature. In addition, as observed in the CD and NMR experiments in the presence of various divalent metal ions, the highly charged DNA might locally destabilize the Cnu structure and modulate the H-NS binding kinetics when a ternary complex is formed.

ACKNOWLEDGMENT

The H-NS plasmid, pHOP11, was kindly provided by Professor Heisaburo Shindo at the Tokyo University of Pharmacy and Life Sciences. We thank Jae-Sun Shin and Kyoung-Seok Ryu for assistance with NMR experiments and Korea Basic Science Institute for use of the 800 and 900 MHz NMR spectrometers.

REFERENCES

1. Blattner, F. R., Plunkett, G., 3rd, Bloch, C. A., Perna, N. T., Burland, V., Riley, M., Collado-Vides, J., Glasner, J. D., Rode, C. K., Mayhew, G. F., Gregor, J., Davis, N. W., Kirkpatrick, H. A., Goeden, M. A., Rose, D. J., Mau, B., and Shao, Y. (1997) The complete genome sequence of *Escherichia coli* K-12, *Science 277*, 1453−1474.
2. Nieto, J. M., Madrid, C., Prenafeta, A., Miquelay, E., Balsalobre, C., Carrascal, M., and Juarez, A. (2000) Expression of the hemolysin operon in *Escherichia coli* is modulated by a nucleoid−protein complex that includes the proteins Hha and H-NS, *Mol. Gen. Genet. 263*, 349−358.
3. Paytubi, S., Madrid, C., Forns, N., Nieto, J. M., Balsalobre, C., Uhlin, B. E., and Juarez, A. (2004) YdgT, the Hha paralogue in *Escherichia coli*, forms heteromeric complexes with H-NS and StpA, *Mol. Microbiol. 54*, 251−263.
4. Kim, M. S., Bae, S. H., Yun, S. H., Lee, H. J., Ji, S. C., Lee, J. H., Srivastava, P., Lee, S. H., Chae, H., Lee, Y., Choi, B. S., Chattoraj, D. K., and Lim, H. M. (2005) Cnu, a Novel oriC-Binding Protein of *Escherichia coli*, *J. Bacteriol. 187*, 6998−7008.
5. Coombes, B. K., Wickham, M. E., Lowden, M. J., Brown, N. F., and Finlay, B. B. (2005) Negative regulation of *Salmonella* pathogenicity island 2 is required for contextual control of virulence during typhoid, *Proc. Natl. Acad. Sci. U.S.A. 102*, 17460−17465.
6. Silphaduang, U., Mascarenhas, M., Karmali, M., and Coombes, B. K. (2007) Repression of intracellular virulence factors in *Salmonella* by the Hha and YdgT nucleoid-associated proteins, *J. Bacteriol. 189*, 3669−3673.
7. Godessart, N., Munoa, F. J., Regue, M., and Juarez, A. (1988) Chromosomal mutations that increase the production of a plasmid-encoded haemolysin in *Escherichia coli*, *J. Gen. Microbiol. 134*, 2779−2787.
8. Mourino, M., Madrid, C., Balsalobre, C., Prenafeta, A., Munoa, F., Blanco, J., Blanco, M., Blanco, J. E., and Juarez, A. (1996) The Hha protein as a modulator of expression of virulence factors in *Escherichia coli*, *Infect. Immun. 64*, 2881−2884.
9. de la Cruz, F., Carmona, M., and Juarez, A. (1992) The Hha protein from *Escherichia coli* is highly homologous to the YmoA protein from *Yersinia enterocolitica*, *Mol. Microbiol. 6*, 3451−3452.
10. Cornelis, G. R. (1994) *Yersinia* pathogenicity factors, *Curr. Top. Microbiol. Immunol. 192*, 243−263.
11. Carmona, M., Balsalobre, C., Munoa, F., Mourino, M., Jubete, Y., De la Cruz, F., and Juarez, A. (1993) *Escherichia coli* hha mutants, DNA supercoiling and expression of the haemolysin genes from the recombinant plasmid pANN202-312, *Mol. Microbiol. 9*, 1011−1018.
12. Nieto, J. M., Mourino, M., Balsalobre, C., Madrid, C., Prenafeta, A., Munoa, F. J., and Juarez, A. (1997) Construction of a double hha hns mutant of *Escherichia coli*: effect on DNA supercoiling and alpha-haemolysin production, *FEMS Microbiol. Lett. 155*, 39−44.
13. Rohde, J. R., Fox, J. M., and Minnich, S. A. (1994) Thermoregulation in *Yersinia enterocolitica* is coincident with changes in DNA supercoiling, *Mol. Microbiol. 12*, 187−199.
14. Balsalobre, C., Juarez, A., Madrid, C., Mourino, M., Prenafeta, A., and Munoa, F. J. (1996) Complementation of the hha mutation in *Escherichia coli* by the ymoA gene from *Yersinia enterocolitica*: dependence on the gene dosage, *Microbiol. 142*, 1841−1846.
15. Atlung, T., and Ingmer, H. (1997) H-NS: a modulator of environmentally regulated gene expression, *Mol. Microbiol. 24*, 7−17.
16. Williams, R. M., and Rimsky, S. (1997) Molecular aspects of the *E. coli* nucleoid protein, H-NS: a central controller of gene regulatory networks, *FEMS Microbiol. Lett. 156*, 175−185.
17. Ueguchi, C., Seto, C., Suzuki, T., and Mizuno, T. (1997) Clarification of the dimerization domain and its functional significance for the *Escherichia coli* nucleoid protein H-NS, *J. Mol. Biol. 274*, 145−151.
18. Yamada, H., Yoshida, T., Tanaka, K., Sasakawa, C., and Mizuno, T. (1991) Molecular analysis of the *Escherichia coli* hns gene encoding a DNA-binding protein, which preferentially recognizes curved DNA sequences, *Mol. Gen. Genet. 230*, 332−336.
19. Spurio, R., Falconi, M., Brandi, A., Pon, C. L., and Gualerzi, C. O. (1997) The oligomeric structure of nucleoid protein H-NS is necessary for recognition of intrinsically curved DNA and for DNA bending, *EMBO J. 16*, 1795−1805.
20. Nieto, J. M., Madrid, C., Miquelay, E., Parra, J. L., Rodriguez, S., and Juarez, A. (2002) Evidence for direct protein−protein interaction between members of the enterobacterial Hha/YmoA and H-NS families of proteins, *J. Bacteriol. 184*, 629−635.
21. Renzoni, D., Esposito, D., Pfuhl, M., Hinton, J. C., Higgins, C. F., Driscoll, P. C., and Ladbury, J. E. (2001) Structural characterization of the N-terminal oligomerization domain of the bacterial chromatin-structuring protein, H-NS, *J. Mol. Biol. 306*, 1127−1137.
22. Dorman, C. J., Hinton, J. C., and Free, A. (1999) Domain organization and oligomerization among H-NS-like nucleoid-associated proteins in bacteria, *Trends Microbiol. 7*, 124−128.
23. Ueguchi, C., Suzuki, T., Yoshida, T., Tanaka, K., and Mizuno, T. (1996) Systematic mutational analysis revealing the functional domain organization of *Escherichia coli* nucleoid protein H-NS, *J. Mol. Biol. 263*, 149−162.
24. Esposito, D., Petrovic, A., Harris, R., Ono, S., Eccleston, J. F., Mbabaali, A., Haq, I., Higgins, C. F., Hinton, J. C., Driscoll, P. C., and Ladbury, J. E. (2002) H-NS oligomerization domain structure reveals the mechanism for high order self-association of the intact protein, *J. Mol. Biol. 324*, 841−850.

25. Smyth, C. P., Lundback, T., Renzoni, D., Siligardi, G., Beavil, R., Layton, M., Sidebotham, J. M., Hinton, J. C., Driscoll, P. C., Higgins, C. F., and Ladbury, J. E. (2000) Oligomerization of the chromatin-structuring protein H-NS, *Mol. Microbiol. 36*, 962−972.
26. Bloch, V., Yang, Y., Margeat, E., Chavanieu, A., Auge, M. T., Robert, B., Arold, S., Rimsky, S., and Kochoyan, M. (2003) The H-NS dimerization domain defines a new fold contributing to DNA recognition, *Nat. Struct. Biol. 10*, 212−218.
27. Cerdan, R., Bloch, V., Yang, Y., Bertin, P., Dumas, C., Rimsky, S., Kochoyan, M., and Arold, S. T. (2003) Crystal structure of the N-terminal dimerisation domain of VicH, the H-NS-like protein of *Vibrio cholerae*, *J. Mol. Biol. 334*, 179−185.
28. Jansson, M., Li, Y. C., Jendeberg, L., Anderson, S., Montelione, B. T., and Nilsson, B. (1996) High-level production of uniformly ^{15}N- and ^{13}C-enriched fusion proteins in *Escherichia coli*, *J. Biomol. NMR 7*, 131−141.
29. Shindo, H., Iwaki, T., Ieda, R., Kurumizaka, H., Ueguchi, C., Mizuno, T., Morikawa, S., Nakamura, H., and Kuboniwa, H. (1995) Solution structure of the DNA binding domain of a nucleoid-associated protein, H-NS, from *Escherichia coli*, *FEBS Lett. 360*, 125−131.
30. Shindo, H., Ohnuki, A., Ginba, H., Katoh, E., Ueguchi, C., Mizuno, T., and Yamazaki, T. (1999) Identification of the DNA binding surface of H-NS protein from *Escherichia coli* by heteronuclear NMR spectroscopy, *FEBS Lett. 455*, 63−69.
31. Clore, G. M., and Gronenborn, A. M. (1994) Multidimensional heteronuclear nuclear magnetic resonance of proteins, *Methods Enzymol. 239*, 349−363.
32. Delaglio, F., Grzesiek, S., Vuister, G. W., Zhu, G., Pfeifer, J., and Bax, A. (1995) NMRPipe: a multidimensional spectral processing system based on UNIX pipes, *J. Biomol. NMR 6*, 277−293.
33. Goddard, T. D., and Kneller, D. G. (2003) Sparky 3, University of California, San Francisco, CA.
34. Cornilescu, G., Delaglio, F., and Bax, A. (1999) Protein backbone angle restraints from searching a database for chemical shift and sequence homology, *J. Biomol. NMR 13*, 289−302.
35. Herrmann, T., Guntert, P., and Wuthrich, K. (2002) Protein NMR structure determination with automated NOE assignment using the new software CANDID and the torsion angle dynamics algorithm DYANA, *J. Mol. Biol. 319*, 209−227.
36. Brunger, A. T., Adams, P. D., Clore, G. M., DeLano, W. L., Gros, P., Grosse-Kunstleve, R. W., Jiang, J. S., Kuszewski, J., Nilges, M., Pannu, N. S., Read, R. J., Rice, L. M., Simonson, T., and Warren, G. L. (1998) Crystallography & NMR system: A new software suite for macromolecular structure determination, *Acta Crystallogr. D: Biol. Crystallogr. 54*, 905−921.
37. Renner, C., Schleicher, M., Moroder, L., and Holak, T. A. (2002) Practical aspects of the 2D ^{15}N-[^{1}h]-NOE experiment, *J. Biomol. NMR 23*, 23−33.
38. Mandel, A. M., Akke, M., and Palmer, A. G., 3rd. (1995) Backbone dynamics of *Escherichia coli* ribonuclease HI: correlations with structure and function in an active enzyme, *J. Mol. Biol. 246*, 144−163.
39. Aurora, R., and Rose, G. D. (1998) Helix capping, *Protein Sci. 7*, 21−38.
40. Mourino, M., Balsalobre, C., Madrid, C., Nieto, J. M., Prenafeta, A., Munoa, F. J., and Juarez, A. (1998) Osmolarity modulates the expression of the Hha protein from *Escherichia coli*, *FEMS Microbiol. Lett. 160*, 225−229.
41. Howard, M. J., Chauhan, H. J., Domingo, G. J., Fuller, C., and Perham, R. N. (2000) Protein−protein interaction revealed by NMR T(2) relaxation experiments: the lipoyl domain and E1 component of the pyruvate dehydrogenase multienzyme complex of *Bacillus stearothermophilus*, *J. Mol. Biol. 295*, 1023−1037.
42. Garcia, J., Cordeiro, T. N., Nieto, J. M., Pons, I., Juarez, A., and Pons, M. (2005) Interaction between the bacterial nucleoid associated proteins Hha and H-NS involves a conformational change of Hha, *Biochem. J. 388*, 755−762.
43. Liu, Q., and Richardson, C. C. (1993) Gene 5.5 protein of bacteriophage T7 inhibits the nucleoid protein H-NS of *Escherichia coli*, *Proc. Natl. Acad. Sci. U.S.A. 90*, 1761−1765.
44. Kajitani, M., and Ishihama, A. (1991) Identification and sequence determination of the host factor gene for bacteriophage Q beta, *Nucleic Acids Res. 19*, 1063−1066.
45. Williams, R. M., Rimsky, S., and Buc, H. (1996) Probing the structure, function, and interactions of the *Escherichia coli* H-NS and StpA proteins by using dominant negative derivatives, *J. Bacteriol. 178*, 4335−4343.
46. Donato, G. M., and Kawula, T. H. (1998) Enhanced binding of altered H-NS protein to flagellar rotor protein FliG causes increased flagellar rotational speed and hypermotility in *Escherichia coli*, *J. Biol. Chem. 273*, 24030−24036.
47. Stella, S., Spurio, R., Falconi, M., Pon, C. L., and Gualerzi, C. O. (2005) Nature and mechanism of the in vivo oligomerization of nucleoid protein H-NS, *EMBO J. 24*, 2896−2905.
48. Rodriguez, S., Nieto, J. M., Madrid, C., and Juarez, A. (2005) Functional replacement of the oligomerization domain of H-NS by the Hha protein of *Escherichia coli*. *J. Bacteriol. 187*, 5452−5459.
49. Yee, A., Chang, X., Pineda-Lucena, A., Wu, B., Semesi, A., Le, B., Ramelot, T., Lee, G. M., Bhattacharyya, S., Gutierrez, P., Denisov, A., Lee, C. H., Cort, J. R., Kozlov, G., Liao, J., Finak, G., Chen, L., Wishart, D., Lee, W., McIntosh, L. P., Gehring, K., Kennedy, M. A., Edwards, A. M., and Arrowsmith, C. H. (2002) An NMR approach to structural proteomics, *Proc. Natl. Acad. Sci. U.S.A. 99*, 1825−1830.
50. Laskowski, R. A., Rullmannn, J. A., MacArthur, M. W., Kaptein, R., and Thornton, J. M. (1996) AQUA and PROCHECK-NMR: programs for checking the quality of protein structures solved by NMR, *J. Biomol. NMR 8*, 477−486.

BI701914T